

# Optical and electrical effects of gold nanoparticles in the active layer of polymer solar cells†

Charlie C. D. Wang,<sup>a</sup> Wallace C. H. Choy,<sup>\*a</sup> Chunhui Duan,<sup>b</sup> Dixon D. S. Fung,<sup>a</sup> Wei E. I. Sha,<sup>a</sup> Feng-Xian Xie,<sup>a</sup> Fei Huang<sup>\*b</sup> and Yong Cao<sup>b</sup>

Received 24th August 2011, Accepted 19th October 2011

DOI: 10.1039/c1jm14150c

The effects of Au nanoparticles (NPs) incorporated into the active layer of polymer solar cells (PSCs) with a newly synthesized donor polymer are investigated in detail. Our work shows that localized surface plasmon resonance (LSPR) introduced by the metallic NPs can experimentally and theoretically enhance the light absorption in the active layer of PSCs because the strong LSPR near field mainly distributes laterally along the active layer. The understanding can be applied to other metallic NP incorporated organic solar cells. Meanwhile, our results show that electrical properties can counterdiminish the optical enhancement from LSPR and thus reduce the overall performance improvement. It is important that both optical and electrical properties need to be studied and optimized simultaneously for achieving improved power conversion efficiency. The study contributes to better understanding the uses of Au NPs for enhancing PSC performances.

## 1. Introduction

Bulk heterojunction (BHJ) polymer solar cells (PSCs) are one of the very promising candidates for photovoltaic devices due to the efficient charge transfer from conjugated polymers to fullerene derivatives.<sup>1,2</sup> Compared with inorganic solar cells, however, one important hindrance for the efficiency improvement of PSCs is the limited light absorption due to the thin active layer limited by the short exciton diffusion length and low carrier mobility.<sup>3–5</sup>

Metallic nanoparticles (NPs) such as Au and Ag NPs and other metallic nanostructures can be potential candidates for improving the light absorption due to the localized surface plasmon resonance (LSPR) which contributes to the significant enhancement of local electromagnetic fields and thus improves the optical properties of the nanostructure devices.<sup>6–11</sup> In addition, the incident photons can be scattered over a longer propagation path in the active layer by metallic nanostructures.<sup>6,12</sup> These features can potentially benefit the light absorption and photocurrent generation of PSCs.

The incorporation of metallic NPs has been explored in PSCs for improving photovoltaic performances.<sup>13–18</sup> However, the contributions of metallic NPs for improving PSC performances

are still not conclusive. For instance, the enhancement of PSC photocurrent by incorporating metallic NPs has been demonstrated experimentally. The enhancement is commonly ascribed to LSPR excitation by using the improvement of incident photon-to-electron conversion efficiency (IPCE).<sup>8,14,15</sup> However, limitations exist in using IPCE as the evidence for the LSPR effect because, apart from optical properties, IPCE is also highly affected by electrical properties such as exciton dissociation, hole and electron transport and collection at their respective electrodes.

In addition, many studies have used the metallic NPs as an interfacial layer on indium tin oxide (ITO)-coated glass substrates or a dopant of buffer layers such as poly(3,4-ethylenedioxythiophene):poly(styrenesulfonate) (PEDOT:PSS).<sup>8,13–16</sup> PSCs with the incorporation of metallic NPs into the active layer, however, have received limited investigation.<sup>17–19</sup> Therefore, the study for further understanding both optical and electrical properties is highly desirable for PSCs with metallic NPs incorporated into the active layer.

In this work, we will demonstrate the impact of the incorporation of monofunctional poly(ethylene glycol) (PEG)-capped Au NPs into the active layer of the polymer blend. A newly synthesized polymer poly[2,7-(9,9-dioctylfluorene)-*alt*-2-((4-(diphenylamino) phenyl)thiophen-2-yl)malononitrile] (PFSDCN) is used as the donor of the active layer. The improvements of open-circuit voltage ( $V_{OC}$ ), short-circuit current ( $J_{SC}$ ) and fill factor (FF) are all obtained with an appropriate amount of Au NPs incorporated into the active layer. As a result, after optimization, the improvement of power conversion efficiency (PCE) by ~32% can be achieved. In order to understand the improvement, we will

<sup>a</sup>Department of Electrical and Electronic Engineering, University of Hong Kong, Pokfulam Road, Hong Kong, China. E-mail: chchoy@eee.hku.hk; Fax: +86 852-2559-8738; Tel: +86 852-2857-8485

<sup>b</sup>Institute of Polymer Optoelectronic Materials & Devices, State Key Laboratory of Physics and Chemistry of Luminescence, South China University of Technology, Guangzhou, 510640, P. R. China. E-mail: msfhuang@scut.edu.cn; Tel: +86-20-8711-4346

† Electronic supplementary information (ESI) available. See DOI: 10.1039/c1jm14150c

experimentally and theoretically investigate the effects of LSPR introduced by Au NPs on the optical properties of PSCs, particularly the PSC active layer. We will also experimentally and theoretically study the effects of Au NPs on PSC electrical properties. The study therefore contributes to better understanding the uses of Au NPs for enhancing PSC performances.

## 2. Experimental

### 2.1 Syntheses of Au NPs and PFSDCN

The syntheses of Au NPs followed the sodium citrate reduction method.<sup>20</sup> After that, 10 mg *O*-[2-(3-mercaptopropionylamino)ethyl]-*O'*-methylpolyethylene glycol (monofunctional PEG,  $M_w$  5000, Sigma-Aldrich) was dissolved in 1 ml de-ionized water, and then the solution was stirred in a rotary evaporator to make it uniform. 0.5 ml Au NPs was added into the solution and then heated at 70 °C for 15 minutes to evaporate the water. Then 0.5 ml chloroform/chlorobenzene (1 : 1, v/v) was added to form well dispersed Au NPs solution. PFSDCN was synthesized *via* a post-functionalized approach by treating its aldehyde-containing precursor polymer, which is prepared by common Suzuki coupling conditions, with malononitrile *via* Knoevenagel reaction under the presence of pyridine. The procedures were similar to what we reported previously,<sup>21</sup> and the detailed information about the synthesis will be reported elsewhere.

### 2.2 Device fabrication

The fabrication process of PEDOT:PSS (Baytron AI 4083) onto ITO-coated glass substrates can be found elsewhere.<sup>22</sup> Before spin-coating the active layer, polymer blend and Au NPs were mixed in the optimized solvent mixture of chloroform/chlorobenzene (1 : 1, v/v ratio) to form uniform solution. The final solution consisted of PFSDCN (2 mg ml<sup>-1</sup>) and [6,6]-phenyl-C<sub>61</sub>butyric acid methyl ester (PCBM, 8 mg ml<sup>-1</sup>, from Nichem Fine Technology Ltd.) and Au NPs with different weight ratios (wt%). The wt% of Au NPs is determined only by considering the weight of PFSDCN. The solution of the polymer blend without Au NPs was also prepared as the control. For the optimized control devices, the mixed solution was spin-coated at 750 rpm for 40 seconds to obtain an active layer with the thickness of ~65 nm as determined by a stylus profiler. The film was then thermally annealed at 100 °C for 10 minutes. Finally, LiF (1 nm)/Al (100 nm) was thermally evaporated as the cathode with a device area of 5.77 mm<sup>2</sup> defined by a shadow mask.

### 2.3 Device characterization

Transmission Electron Microscope (TEM) images of Au NPs were measured using a Philips Tecnai G2 20 S-TWIN. The cross-sectional images of the PSCs were taken by a Hitachi S-4800 field emission scanning electron microscope (SEM). The absolute refractive index and absorption coefficient were measured by Woollam spectroscopic ellipsometry. The current density–voltage ( $J$ – $V$ ) measurement can be found elsewhere.<sup>22</sup> The IPCE measurement was performed by a system combining a xenon lamp, a monochromator, a chopper and a lock-in amplifier together with a calibrated silicon photodetector. Atomic force

microscope (AFM) characterization was conducted by using a Nanoscope III (Digital Instrument) in the tapping mode.

## 2.4 Theoretical modelling

In order to investigate the effects of Au NPs on the light absorption at the active layer of PSCs, the light absorption of the active layer, which determines the exciton generation rate, has been theoretically determined. As a rigorous, fast and efficient solver of Maxwell's equation, volume integral equation-fast Fourier transform (VIE-FFT) has been built in this work. The algorithm is particularly capable of modelling thin-film solar cells incorporating plasmonic NPs of size ranging from 10 nm to 100 nm. The plasmon coupling and hybridization of NPs, as well as their interplay with the PSC device structure, have been fully taken into account. We have also theoretically studied the electrical properties of PSCs by solving the organic semiconductor equations involving Poisson, drift-diffusion, and continuity equations.<sup>23,24</sup> Details of the optical and electrical models are described in ESI B and C† respectively.

## 3. Results and discussion

### 3.1 Overall experimental results

The absorption spectrum of PFSDCN film is shown in Fig. 1 and has two absorption peaks at around 374 nm and 518 nm. The chemical structure of PFSDCN is shown in the inset of Fig. 1. The optical bandgap and oxidation potential of PFSDCN are 2.05 eV and 0.91 V, respectively. The highest occupied molecular orbital (HOMO) is –5.32 eV as measured by the cyclic voltammetry (CV) method and the lowest unoccupied molecular orbital (LUMO) is –3.27 eV calculated from the HOMO level and optical bandgap. The absorption spectrum of Au NPs in chloroform/chlorobenzene (1 : 1, v/v ratio) is shown in Fig. 2 with the peak at ~520 nm. The average diameter of Au NPs is ~18 nm determined from TEM measurement (inset of Fig. 2). The current density ( $J$ ) *versus* voltage ( $V$ ) characteristics are shown in Fig. 3a. The effects of Au NPs concentration on PSC performances including  $V_{OC}$ ,  $J_{SC}$ , FF and PCE are shown in Fig. 3b(i)–(iv) respectively. It should be noted that the fabrication conditions such as the ratio of PFSDCN to PCBM, spin-coating speed and time, annealing temperature and duration have been optimized for the control devices before the addition of Au NPs.

It is observed that Au NPs with a low concentration of 0.5 wt% improve  $V_{OC}$  and  $J_{SC}$ . However, both  $V_{OC}$  and  $J_{SC}$  reduce when

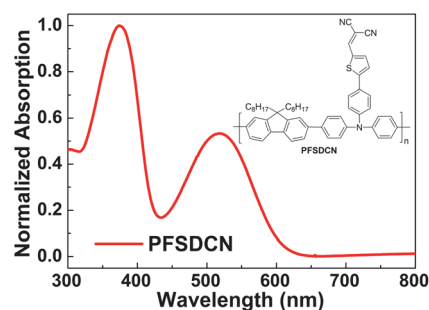
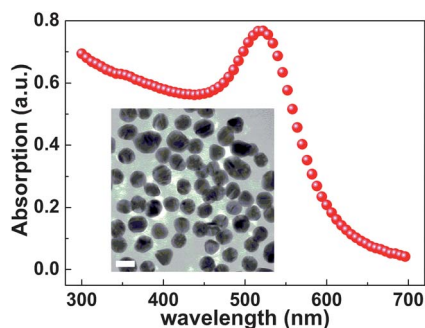
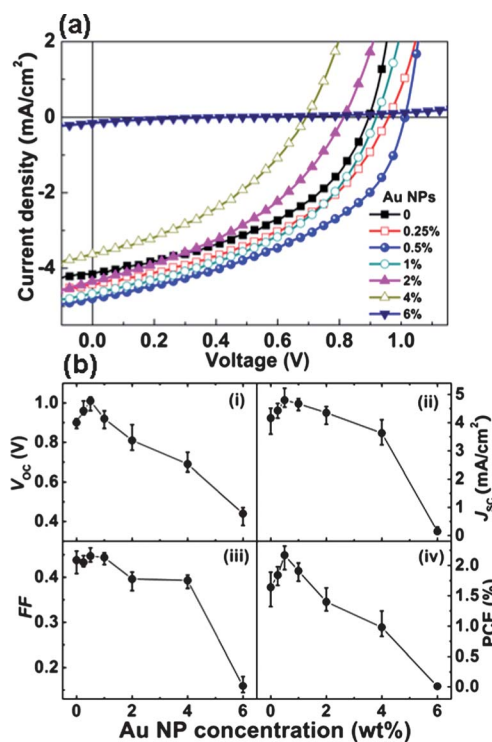


Fig. 1 The normalized absorption spectrum and chemical structure of PFSDCN.



**Fig. 2** The absorption spectrum of Au NPs in chloroform/chlorobenzene (1 : 1 volume ratio) with the peak at  $\sim 520$  nm. The inset is the TEM image of Au NPs. The white colour bar is 20 nm long.



**Fig. 3** (a) The current–voltage characteristics of the representative PSCs incorporated with different NP concentrations under AM 1.5G illumination at  $100 \text{ mW cm}^{-2}$ . (b) Electrical parameters of NP incorporated PSCs: (i)  $V_{oc}$ ; (ii)  $J_{sc}$ ; (iii) FF and (iv) PCE.

Au NPs concentration increases further. FF increases slightly and then decreases as Au NPs concentration increases. From the dark  $J$ – $V$  characteristics (ESI A: Fig. SA1†), the electrical conductivity improves by adding Au NPs, which is in agreement with others reports.<sup>17</sup> The difference here is that the electrical conductivity reduces with the further increase of Au NPs concentration  $> 2$  wt%. Consequently, PCE is improved by  $\sim 32\%$  from 1.64% (without Au NPs) to 2.17% (with 0.5 wt% Au NPs), and then decreases. When Au NPs concentration reaches 6 wt%, almost no photovoltaic effect is observed (PCE  $\approx 0.01\%$ ).

It should be noted that in the study, Au NPs have been capped with PEG. In order to investigate the effects of PEG on device performances, the PEG-only PSCs were fabricated in which only PEG was incorporated into the polymer blend. PEG

concentration in the mixed solution is  $\sim 0.08 \text{ mg ml}^{-1}$  which equals that of the PEG in 0.5 wt% Au NPs mixed with polymer blend solution. As shown in ESI A (Fig. SA2†), the PEG-only PSC shows similar  $J$ – $V$  characteristics and PCE ( $\sim 1.67\%$ ) to that of the device without PEG incorporation (PCE  $\approx 1.64\%$ ). Therefore, PEG itself is not likely to have pronounced effects on device performances.

### 3.2 LSPR effects

To verify the degree of contributions of the LSPR effect, we measure the absorption spectrum of the active layer incorporated with various Au NP concentrations. Meanwhile, to understand the physics, we build a model to rigorously solve Maxwell's equations and study the absorption of PSCs as shown in Fig. 4. The theoretical near-field profile of electric field (Fig. 4b) shows very strong field strength laterally distributed along the active layer which can enhance the light absorption by the polymer blend for generating carriers. It is noteworthy that when Au NPs are incorporated into the PEDOT:PSS layer (*i.e.* the layer adjacent to the active layer), the light absorption in the active layer is not clearly enhanced due to the lateral distribution feature of the strong LSPR near field along the PEDOT:PSS layer rather than a vertical distribution into the active layer as described in our other work.<sup>25</sup>

The theoretical and experimental absorption enhancements of the active layer (PFSDCN:PCBM) indicate that LSPR for the case of low Au NPs concentration mixed active layer exists at around 650 nm which is different from that of Au NPs ( $\sim 520$  nm) in chloroform/chlorobenzene (1 : 1, v/v ratio) due to the change of the surrounding optical environment. Moreover, when the spacing between Au NPs reduces (*i.e.* higher Au NPs concentration), the theoretical and experimental results show that the resonance strength increases and slightly red shifts. Consequently, the theoretical results are in agreement with our experimental results. Our results demonstrate and explain the features of LSPR excited by Au NPs incorporated into the PSCs active layer.

The light absorption can be enhanced experimentally by over 100% at the resonance region when Au NPs concentration increases to 6 wt% as shown in Fig. 4a. However, the effects of LSPR alone cannot completely interpret the overall observed phenomena of PSCs. For example, low Au NPs concentration can benefit PSC performances. Continuously enhanced light absorption is obtained with the increase of Au NPs

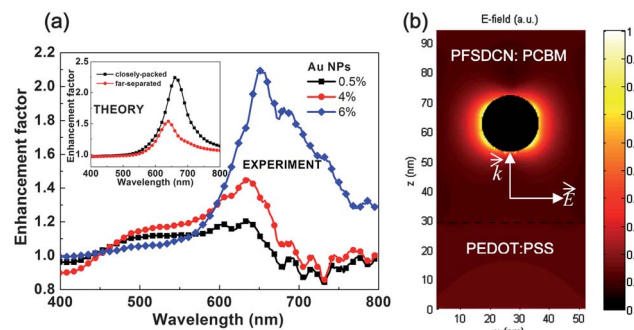


**Fig. 4** (a) Experimental and theoretical (inset) absorbance enhancement factor of the active layer with different amounts of Au NPs. (b) Theoretical near field distribution around an Au NP in the active layer.

concentration due to the stronger LSPR. However, when Au NPs concentration  $> 0.5$  wt%, deterioration of device performances is obtained, which is quite unexpected in the viewpoint of LSPR effects. This can be further illustrated from IPCE characteristics as shown in Fig. 5. When the Au NPs concentration reaches 6 wt%, a large absorption enhancement factor is obtained (Fig. 4a), but IPCE decreases to almost zero. Therefore, besides LSPR effects, the effects of Au NPs on PSC electrical properties need to be investigated for understanding the results.

### 3.3 Effects on carrier mobility

Generally, electron and hole mobilities are important factors and should be high enough to guarantee a large carrier hopping rate, to avoid carrier recombination and to prevent the build up of space charge.<sup>26,27</sup> For Au NP incorporated PSCs, we make hole-only and electron-only devices for determining the hole and electron mobility, respectively, by fitting from the dark  $J$ - $V$  curves using the space-charge limited current (SCLC) model.<sup>28</sup> Hole-only devices have structures of the ITO/PEDOT:PSS/polymer blend: Au NPs/Au (20 nm)/Al (80 nm). It has been reported that the work function of ITO can be effectively modified for electron collection in inverted PSCs by evaporating 1 nm of Ca.<sup>29,30</sup> For our electron-only devices, we adopt this method and use the structure of ITO/Ca (2 nm)/polymer blend: Au NPs/LiF (1 nm)/Al (100 nm). The mobility of holes and electrons is shown in Fig. 6 and the detailed experimental data and fitting curves are discussed in ESI A (Fig. SA4†). The hole mobility ( $1.18$ – $4.25 \times 10^{-4} \text{ cm}^2 \text{ V}^{-1} \text{ s}^{-1}$ ) is about one order less than electron mobility ( $0.78$ – $1.2 \times 10^{-3} \text{ cm}^2 \text{ V}^{-1} \text{ s}^{-1}$ ) except for that of PSC with 6 wt% Au NPs (Fig. 6). In addition, the trend of PSC electrical conductivity *versus* Au NPs concentration (ESI A: Fig. SA1†) is consistent with that of hole mobility. Hence, the charge transport of our devices is dominantly limited by the hole transport property, which agrees well with the fact that the transport process in the organic materials is dominated by the slow charge carriers.<sup>23</sup>

The effects of Au NPs on the carrier mobility are manifold. On one hand, Au NPs can introduce dopant states within the bandgap of polymer which can provide hopping sites for holes and thus enhance the mobility.<sup>17</sup> In fact, the metallic NP-induced energy levels for holes have also been reported previously in a hybrid Ag NPs/organic resonant tunnelling diode.<sup>31</sup> On the other hand, the incorporated Au NPs will modify the nanoscale morphology of the polymer/fullerene blend, especially with high NPs concentration,

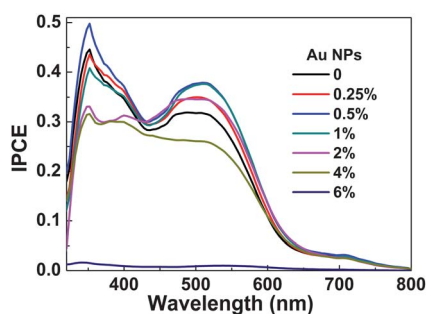


Fig. 5 IPCE of PSCs incorporated with different concentrations of Au NPs.

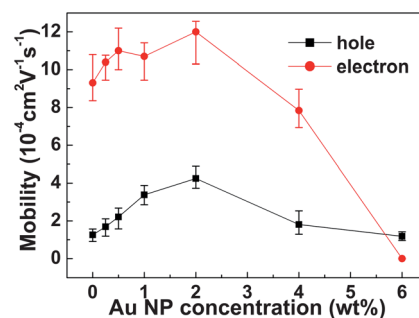


Fig. 6 Effects of Au NP concentration on the hole and electron mobilities in the active layer.

which can be evidenced by the AFM image as shown in Fig. 7. The root mean square (RMS) roughness of the active layer increases significantly from  $\sim 0.617$  nm (without Au NPs) to  $\sim 8.062$  nm (6 wt% Au NPs) and an obvious different surface morphology is observed. In addition, the phase image shows a much larger contrast for the active layer film with 6 wt% Au NPs, indicating a nanoscale morphology change of the blends.<sup>32,33</sup> Such a NP-induced nanoscale morphology change may not favor charge transport and thus degrades the carrier mobility. The two factors will therefore compete with each other in our devices.

At low Au NPs concentration, the blend morphology does not have clear changes from our AFM results (*i.e.* RMS only increases to  $\sim 1.204$  nm for 1 wt% Au NP incorporation; figure is not shown here) and therefore only plays a less important role in modifying carrier mobility. As a result, with low Au NPs concentration, the increases of carrier mobility should be explained by the introduction of hopping sites for holes. These hopping sites are expected to have greater influence on hole mobility than electron mobility, which agrees well with the experimental results. Compared with the control devices (without Au NPs), incorporation with 2 wt% Au NPs contributes to an improvement of hole mobility by  $\sim 237\%$  (from  $1.26 \times 10^{-4} \text{ cm}^2 \text{ V}^{-1} \text{ s}^{-1}$  to  $4.25 \times 10^{-4} \text{ cm}^2 \text{ V}^{-1} \text{ s}^{-1}$ ), and an improvement of electron mobility only by  $\sim 28\%$  (from  $0.93 \times 10^{-3} \text{ cm}^2 \text{ V}^{-1} \text{ s}^{-1}$  to  $1.2 \times 10^{-3} \text{ cm}^2 \text{ V}^{-1} \text{ s}^{-1}$ ). With high Au NPs concentration, the NP-induced morphology change dominates the charge transport process and thus both the hole and electron mobility are expected to be degraded, which is consistent with the experimental results as shown in Fig. 6.

Therefore, the enhanced carrier mobilities with the proper amount of Au NPs can partly account for the improved photocurrent generation and FF due to the improved carrier collection and the reduced bulk resistance. It is noted that the device performances, *i.e.*  $J_{SC}$  and PCE begin to decrease when Au NPs concentration  $\geq 1$  wt% although the carrier mobility keeps on maintaining increment until the Au NPs concentration reaching 2 wt%. This indicates that besides the carrier mobility, Au NPs should affect other operation processes of PSCs. One process likely to be affected is the dissociation of excitons to free carriers as described below.

### 3.4 Effects on exciton dissociation

To investigate the efficiency of exciton dissociation, photocurrent ( $J_{ph}$ ) as a function of effective voltage ( $V_{EFF}$ ) is measured



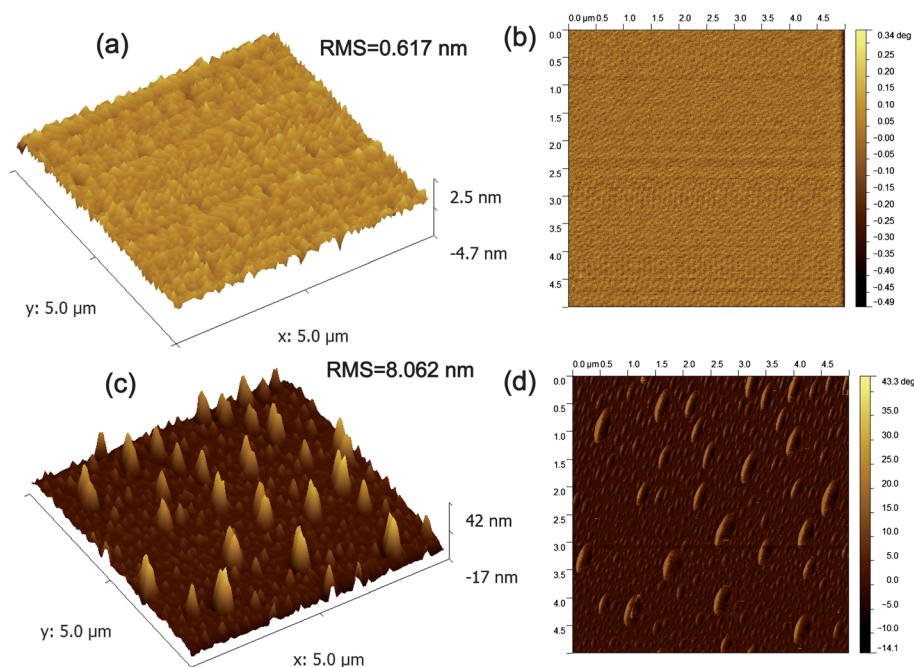


**Fig. 7** AFM images of the active layer: (a) height image, RMS = 0.617 nm and (b) phase image of the active layer film without Au NPs; (c) height image, RMS = 8.062 nm and (d) phase image of the active layer film with Au NPs; 6 wt%.

and fitted following Mihailetchi *et al.*<sup>34</sup> The  $J_{\text{ph}} \approx V_{\text{EFF}}$  features and the corresponding fitting curves are shown in ESI A: Fig. SA5†. The maximal generation rate of excitons ( $G_{\text{max}}$ ) for all the samples is obtained to be on the order of  $5 \times 10^{27} \text{ m}^{-3} \text{ s}^{-1}$ . The exciton decay rate ( $k_{\text{F}}$ ) and exciton dissociation probability ( $P_{\text{exc}}$ ) under short-circuit condition are shown in Fig. 8. It can be observed that Au NPs indeed affect the exciton dissociation. Low Au NPs concentration makes  $k_{\text{F}}$  reduce and  $P_{\text{exc}}$  increase slightly from  $\sim 76\%$  to  $\sim 80\%$ . While Au NPs concentration further increases,  $P_{\text{exc}}$  reduces.

The slight enhancement of  $P_{\text{exc}}$  at low Au NPs concentration can be attributed to the excitation of LSPR<sup>14</sup> and the enhanced hole mobility which reduces the carrier back-transfer induced recombination.<sup>23,26</sup> The degradation of exciton dissociation efficiency at high NPs concentration can be attributed to the morphology change of the active layer and the reduced  $V_{\text{OC}}$ . As indicated from the surface image of the active layer in Fig. 7, the nanoscale morphology change inside the active layer is significant especially at high NPs concentration. Such a NP-induced morphology change may make the polymer blend less favourable

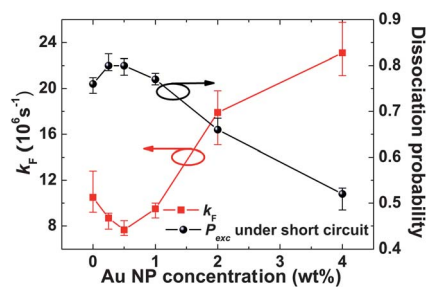


**Fig. 8** Effects of Au NP concentration on the decay rate of bound electron-hole pair ( $k_{\text{F}}$ ) (square) and exciton dissociation probability ( $P_{\text{exc}}$ ) under short circuit condition (circle).

for exciton dissociation. On the other hand, the reduction of  $V_{\text{OC}}$  means a decrease of built-in electric field in the active layer, which will make the exciton dissociation process less efficient since the exciton dissociation is very field-dependent.<sup>5</sup>

### 3.5 $V_{\text{OC}}$

As Au NPs concentration increases,  $V_{\text{OC}}$  first increases from  $\sim 0.90 \text{ V}$  (without Au NPs) to  $\sim 1.01 \text{ V}$  (Au NPs: 0.5 wt%) and then decreases. When Au NPs concentration increases to 6 wt%,  $V_{\text{OC}}$  reduces significantly to 0.44 V. In BHJ PSCs, charge recombination is commonly regarded as one important loss mechanism limiting  $V_{\text{OC}}$ .<sup>35,36</sup> With a proper amount of Au NPs ( $\leq 0.5\%$ ), the reduced recombination due to the enhanced carrier mobility and exciton dissociation is expected to improve  $V_{\text{OC}}$ . To understand the contribution of recombination reduction to  $V_{\text{OC}}$ , a theoretical model is built based on the fundamental equations describing carrier transports in semiconductors following Koster *et al.*<sup>23</sup> Details of the model can be found in ESI C†. In modeling, the device parameters for PSCs with various Au NPs such as carrier mobilities and  $k_{\text{F}}$  are obtained from the methods discussed in Part 3.3 and 3.4 above while other parameters remained constant. The results show that  $V_{\text{OC}}$  has almost no change, suggesting that the reduced recombination due to increased carrier mobilities does not contribute to the  $V_{\text{OC}}$  improvement. An alternative explanation for the  $V_{\text{OC}}$  improvement with Au NPs incorporation ( $\leq 0.5 \text{ wt}\%$ ) is the downward shift of the donor HOMO level due to the reduced polarization energy.<sup>37,38</sup> Downward shift of the donor HOMO level by 0.1 eV is best fitted as shown in ESI C: Fig. SC1†, for the increase of the measured  $V_{\text{OC}}$  by  $\sim 0.1 \text{ V}$  for the 0.5 wt% Au NP case.

The degradation of  $V_{\text{OC}}$  at high Au NPs concentration is due to several factors. At high concentration, a large amount of Au NPs may modify the interfacial charge states at the cathode and

even break down the Fermi level pinning between the cathode metal and the fullerene reduction potential, which can downward shift the cathode work function and lead to remarkable  $V_{OC}$  reduction. This can be further revealed by the SEM cross-sectional images of the active layer in Fig. SA6†. With low concentration of Au NPs (0.5 wt% and 2 wt%), the Au NPs are mostly located near the bottom of PFSDCN:PCBM (near to the interface with PEDOT:PSS). When embedding a high concentration of Au NPs (6 wt%, Fig. SA6(c)†), aggregation of NPs is observed and some are located at the surface of the active layer, which induces a significant morphology change and  $V_{OC}$  reduction. Our theoretical results show that the change of work function of the cathode causes the reduction of  $V_{OC}$ . When the cathode work function is downward shifted by 0.56 eV,  $V_{OC}$  reduces to 0.69 V for PSCs with 4 wt% of Au NPs concentration (Fig. SC1†). The other subordinate factor resulting in  $V_{OC}$  reduction is that more shunt paths are induced by the Au NPs, which can be well indicated from the increased reverse current for the PSCs as the concentration of Au NPs increases (see ESI A: Fig. SA1†). The shunt paths formed directly from anode to cathode are believed to reduce the  $V_{OC}$ .<sup>39,40</sup>

#### 4. Conclusions

In this study, the effects of monofunctional PEG-capped Au NPs (0.5 wt%) on PSCs have been theoretically and experimentally investigated by introducing the Au NPs into the blend of newly synthesized polymer of PFSDCN and PCBM. Our results show that due to the interesting feature of the strong lateral distribution of LSPR near field along the active layer, light absorption is enhanced by incorporating Au NPs into the active layer. The understanding can be applied to other metallic NP incorporated organic solar cells. Meanwhile, our results show that electrical properties can counter-diminish the optical enhancement from LSPR which reduces the overall performance improvement. It is important that both optical and electrical properties need to be studied and optimized simultaneously. Our results show that after optimization, power conversion efficiency can be improved by ~32%. The study contributes to better understanding the uses of Au NPs for enhancing PSC performances.

#### Acknowledgements

This work is supported by UGC grant (#400897) of the University of Hong Kong and Hong Kong Research Grants Council (HKU#712108 and HKU#712010) from the Research Grants Council of the HK Special Administrative Region, China. Huang would like to acknowledge the financial support from the Natural Science Foundation of China (no. 50990065, 51010003, 51073058 and 20904011), the Ministry of Science and Technology, China (MOST) National Research Project (no. 2009CB623601) and the Fundamental Research Funds for the Central Universities, South China University of Technology (no. 2009220012).

#### References

1 G. Yu, J. Gao, J. C. Hummelen, F. Wudl and A. J. Heeger, *Science*, 1995, **270**, 1789.

- C. J. Brabec, G. Zerza, G. Cerullo, S. De Silvestri, S. Luzzati, J. C. Hummelen and S. Sariciftci, *Chem. Phys. Lett.*, 2001, **340**, 232.
- D. Wöhrle and D. Meissner, *Adv. Mater.*, 1991, **3**, 129.
- V. Shrotriya, E. H.-E. Wu, G. Li, Y. Yao and Y. Yang, *Appl. Phys. Lett.*, 2006, **88**, 064104.
- P. W. M. Blom, V. D. Mihailetschi, L. J. A. Koster and D. E. Markov, *Adv. Mater.*, 2007, **19**, 1551.
- H. A. Atwater and A. Polman, *Nat. Mater.*, 2010, **9**, 205.
- J. R. Cole and N. J. Halas, *Appl. Phys. Lett.*, 2006, **89**, 153120.
- S.-S. Kim, S.-I. Na, J. Jo, D.-Y. Kim and Y.-C. Nah, *Appl. Phys. Lett.*, 2008, **93**, 073307.
- C. Min, J. Li, G. Veronis, J.-Y. Lee, S. Fan and P. Peumans, *Appl. Phys. Lett.*, 2010, **96**, 133302.
- W. E. I. Sha, W. C. H. Choy and W. C. Chew, *Opt. Lett.*, 2011, **36**, 478.
- W. E. I. Sha, W. C. H. Choy and W. C. Chew, *Opt. Express*, 2010, **18**, 5993.
- Y. A. Akimov, W. S. Koh, S. Y. Sian and S. Ren, *Appl. Phys. Lett.*, 2010, **96**, 073111.
- J.-L. Wu, F.-C. Chen, Y.-S. Hsiao, F.-C. Chien, P. Chen, C.-H. Kuo, M. H. Huang and C.-S. Hsu, *ACS Nano*, 2011, **5**, 959.
- F.-C. Chen, J.-L. Wu, C.-L. Lee, Y. Hong, C.-H. Kuo and M. H. Huang, *Appl. Phys. Lett.*, 2009, **95**, 013305.
- A. J. Morfa, K. L. Rowlen, T. H. Reilly, III, M. J. Romero and J. van de Lagemaat, *Appl. Phys. Lett.*, 2008, **92**, 013504.
- W.-J. Yoon, K.-Y. Jung, J. Liu, T. Duraisamy, R. Revur, F. L. Teixeira, S. Sengupta and P. R. Berger, *Sol. Energy Mater. Sol. Cells*, 2010, **94**, 128.
- K. Kim and D. L. Carroll, *Appl. Phys. Lett.*, 2005, **87**, 203113.
- B. V. K. Naidu, J. S. Park, S. C. Kim, S.-M. Park, E.-J. Lee, K.-J. Yoon, S. J. Lee, J. W. Lee, Y.-S. Gal and S.-H. Jin, *Sol. Energy Mater. Sol. Cells*, 2008, **92**, 397.
- K. Topp, H. Borchert, F. Johnen, A. V. Tunc, M. Knipper, E. von Hauff, J. Parisi and K. Al-Shamery, *J. Phys. Chem. A*, 2009, **114**, 3981.
- S. Link and M. A. El-Sayed, *J. Phys. Chem. B*, 1999, **103**, 4212.
- C. Duan, W. Cai, F. Huang, J. Zhang, M. Wang, T. Yang, C. Zhong, X. Gong and Y. Cao, *Macromolecules*, 2010, **43**, 5262.
- C.-D. Wang and W. C. H. Choy, *Sol. Energy Mater. Sol. Cells*, 2011, **95**, 904.
- L. J. A. Koster, E. C. P. Smits, V. D. Mihailetschi and P. W. M. Blom, *Phys. Rev. B: Condens. Matter Mater. Phys.*, 2005, **72**, 085205.
- D. W. Sievers, V. Shrotriya and Y. Yang, *J. Appl. Phys.*, 2006, **100**, 114509.
- D. D. S. Fung, L. Qiao, W. C. H. Choy, C.-D. Wang, W. E. I. Sha, F.-X. Xie and S. He, *J. Mater. Chem.*, 2011, **21**, 16349.
- A. C. Mayer, S. R. Scully, B. E. Hardin, M. W. Rowell and M. D. McGehee, *Mater. Today*, 2007, **10**, 28.
- M. M. Mandoc, L. J. A. Koster and P. W. M. Blom, *Appl. Phys. Lett.*, 2007, **90**, 133504.
- V. D. Mihailetschi, J. K. J. van Duren, P. W. M. Blom, J. C. Hummelen, R. A. J. Janssen, J. M. Kroon, M. T. Rispen, W. J. H. Verhees and M. M. Wienk, *Adv. Funct. Mater.*, 2003, **13**, 43.
- D. W. Zhao, P. Liu, X. W. Sun, S. T. Tan, L. Ke and A. K. K. Kyaw, *Appl. Phys. Lett.*, 2009, **95**, 153304.
- C. Y. Jiang, X. W. Sun, D. W. Zhao, A. K. K. Kyaw and Y. N. Li, *Sol. Energy Mater. Sol. Cells*, 2010, **94**, 1618.
- T. Zheng, W. C. H. Choy and Y. Sun, *Adv. Funct. Mater.*, 2009, **19**, 2648.
- H.-Y. Chen, J. Hou, S. Zhang, Y. Liang, G. Yang, Y. Yang, L. Yu, Y. Wu and G. Li, *Nat. Photonics*, 2009, **3**, 649.
- Z. Xu, L.-M. Chen, G. Yang, C.-H. Huang, J. Hou, Y. Wu, G. Li, C.-S. Hsu and Y. Yang, *Adv. Funct. Mater.*, 2009, **19**, 1227.
- V. D. Mihailetschi, L. J. A. Koster, J. C. Hummelen and P. W. M. Blom, *Phys. Rev. Lett.*, 2004, **93**, 216601.
- C. J. Brabec, A. Cravino, D. Meissner, N. S. Sariciftci, T. Fromherz, M. T. Rispen, L. Sanchez and J. C. Hummelen, *Adv. Funct. Mater.*, 2001, **11**, 374.
- K. Vandewal, K. Tvingstedt, A. Gadisa, O. Inganäs and J. V. Manca, *Nat. Mater.*, 2009, **8**, 904.
- K. Akaike, K. Kanai, Y. Ouchi and K. Seki, *Adv. Funct. Mater.*, 2010, **20**, 715.
- W. Tress, K. Leo and M. Riede, *Adv. Funct. Mater.*, 2011, **21**, 2140.
- H. J. Snaith, N. C. Greenham and R. H. Friend, *Adv. Mater.*, 2004, **16**, 1640.
- B. Sun, H. J. Snaith, A. S. Dhoot, S. Westenhoff and N. C. Greenham, *J. Appl. Phys.*, 2005, **97**, 014914.